Breaking crosstalk limits to dynamic holography using orthogonality of high-dimensional random vectors
SUPPLEMENTARY INFORMATION

Ghaith Makey[1,2], Özgün Yavuz[3], Denizhan K. Kesim[3], Ahmet Turnalı[3], Parviz Elahi[1,2], Serim Ilday[1], Onur Tokel[1,2,†], F. Ömer Ilday[1,2,3,†]

[1] UNAM – National Nanotechnology Research Center and Institute of Materials Science and Nanotechnology, Bilkent University, Ankara, 06800, Turkey
[2] Department of Physics, Bilkent University, Ankara, 06800, Turkey
[3] Department of Electrical and Electronics Engineering, Bilkent University, Ankara, 06800, Turkey
[†]Corresponding authors. E-mail: otokel@bilkent.edu.tr (O.T.), ilday@bilkent.edu.tr (F.Ö.I.)

Adaptive-additive IFTA

The algorithm is based on adaptive-additive IFTA, which is an improvement over Grechberg-Saxton algorithm[1]. In order to create images with high fidelity, the phase of the source image is changed at each IFTA iteration. For further optimisation, the amplitude of the source image is changed to the weighted addition of the source itself and the image of the generated hologram at that iteration. The number of iterations per image is decided based on the value of Root Mean Square Error (RMSE) for that image. The code was executed using the parallel computing capability of MATLAB on a graphics processing unit.

Incorporation of occlusion cues

It is well known that occlusion, *i.e.*, blocking of objects in the background by those in the foreground, cannot natively be achieved with holography since light fields cannot block each other. However, our method can optionally be used with a 3D rendering technique to adaptively adjust the projection to create impression of occlusion based on the observer's position with respect to the projection of the hologram. To demonstrate this possibility, we built a scene of 3D objects using a 3D software (Supplementary Fig. 11a). Then, we exported the 200-slices of the scene with each slice illuminated according to the camera position. These 200 slices were processed using our method to generate an 8K hologram. In Supplementary Fig. 11b-d, we show the simulated projections corresponding to three different positions of the observer, demonstrating incorporation of occlusion cues. The main limitation of our adaptive approach is that it works only for a single observer at a given moment. Alternative techniques for incorporation of occlusions cues have been proposed[2-4], which can similarly be combined with our method following appropriate modifications.

Supplementary Figures

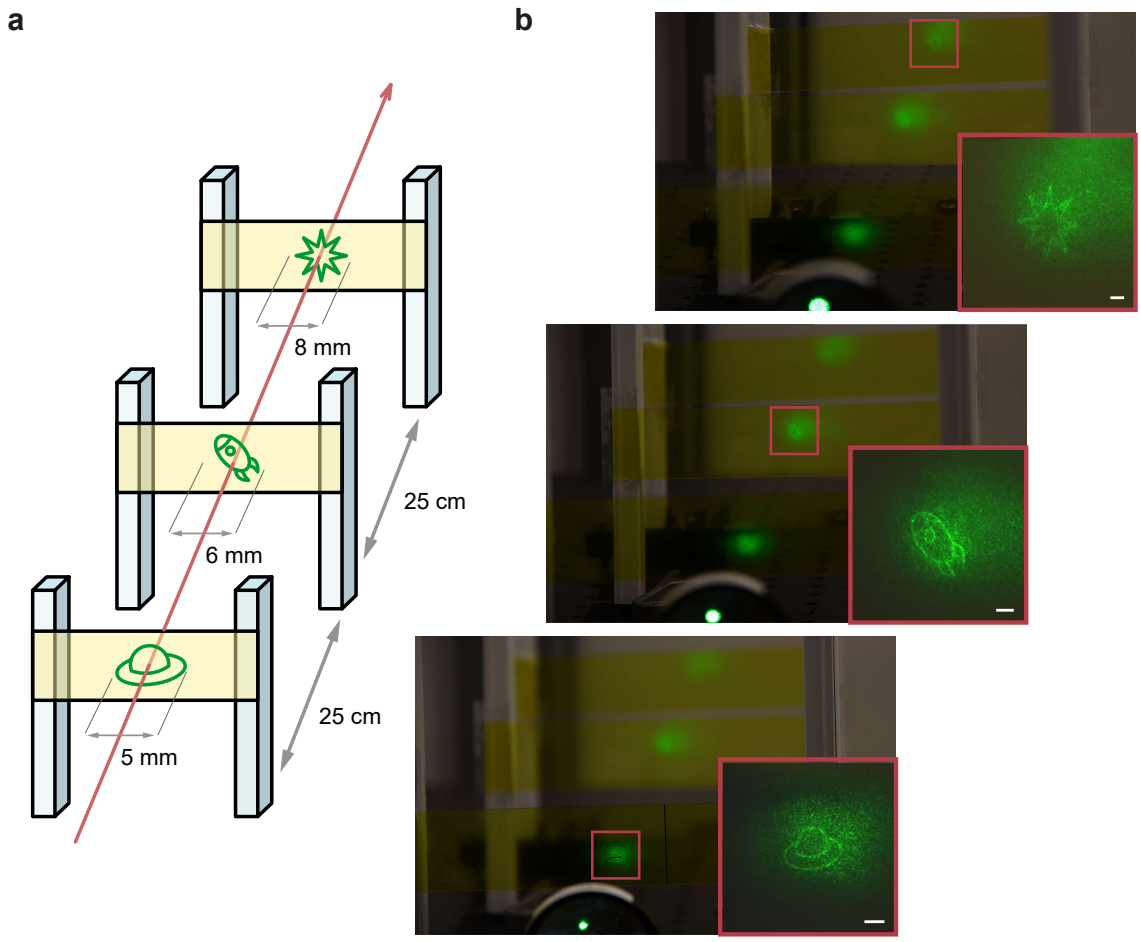

Supplementary Figure 1 Prototype of an extremely low-cost dynamic 3D display operating at visible wavelengths. (a) Experimental scheme for reconstructing the 3-plane projection from a Fresnel hologram. The hologram (512 × 512 pixels) is implemented on an SLM which was extracted from a "budget-grade" projector, and is illuminated with 520 nm green light. **(b)** The 3D Fresnel hologram forms 3 back-to-back images; a flying disc, a space shuttle, and a star symbol. The distances from the SLM are 70, 95, and 120 cm. Inset: Close-up view. Scale bar, 2 mm.

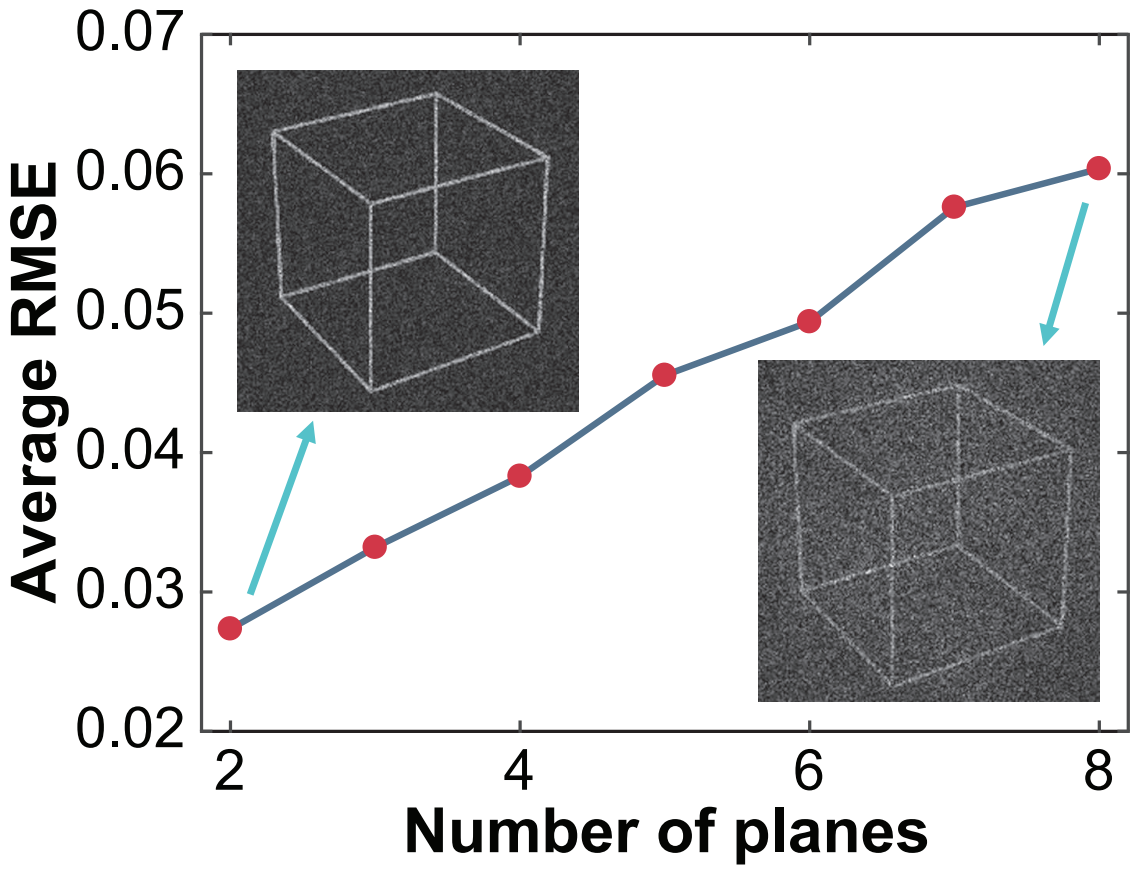

Supplementary Figure 2 Image quality characterisation of 3D Fresnel CGHs. Calculated average RMSE for seven sets of 3D holograms, each projecting to a different number of planes. The insets show representative images for 2- and 8-plane projecting Fresnel CGHs, respectively, providing visual assistance in evaluating image quality.

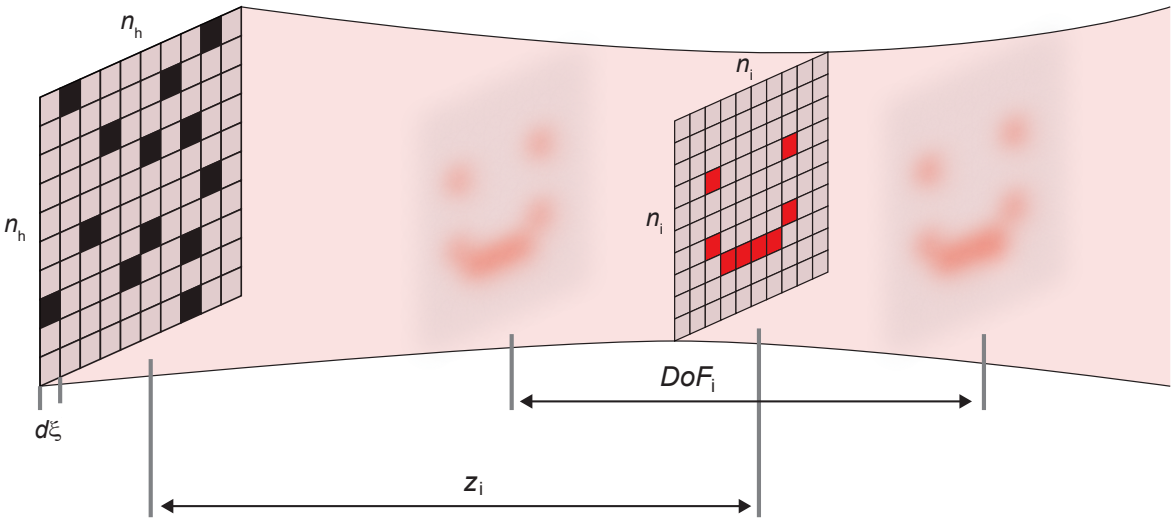

Supplementary Figure 3 Depth-of-field at image plane *i*. Relevant parameters for calculating the depth-of-field at plane i (DoF_i) are, (i) the pixel size of the hologram ($d\xi$), (ii) number of pixels of the hologram and the image, and (iii) focal length z_i at which the image is projected. The hologram has $n_h \times n_h$ pixels, and the resolution of the image at plane i is $n_i \times n_i$.

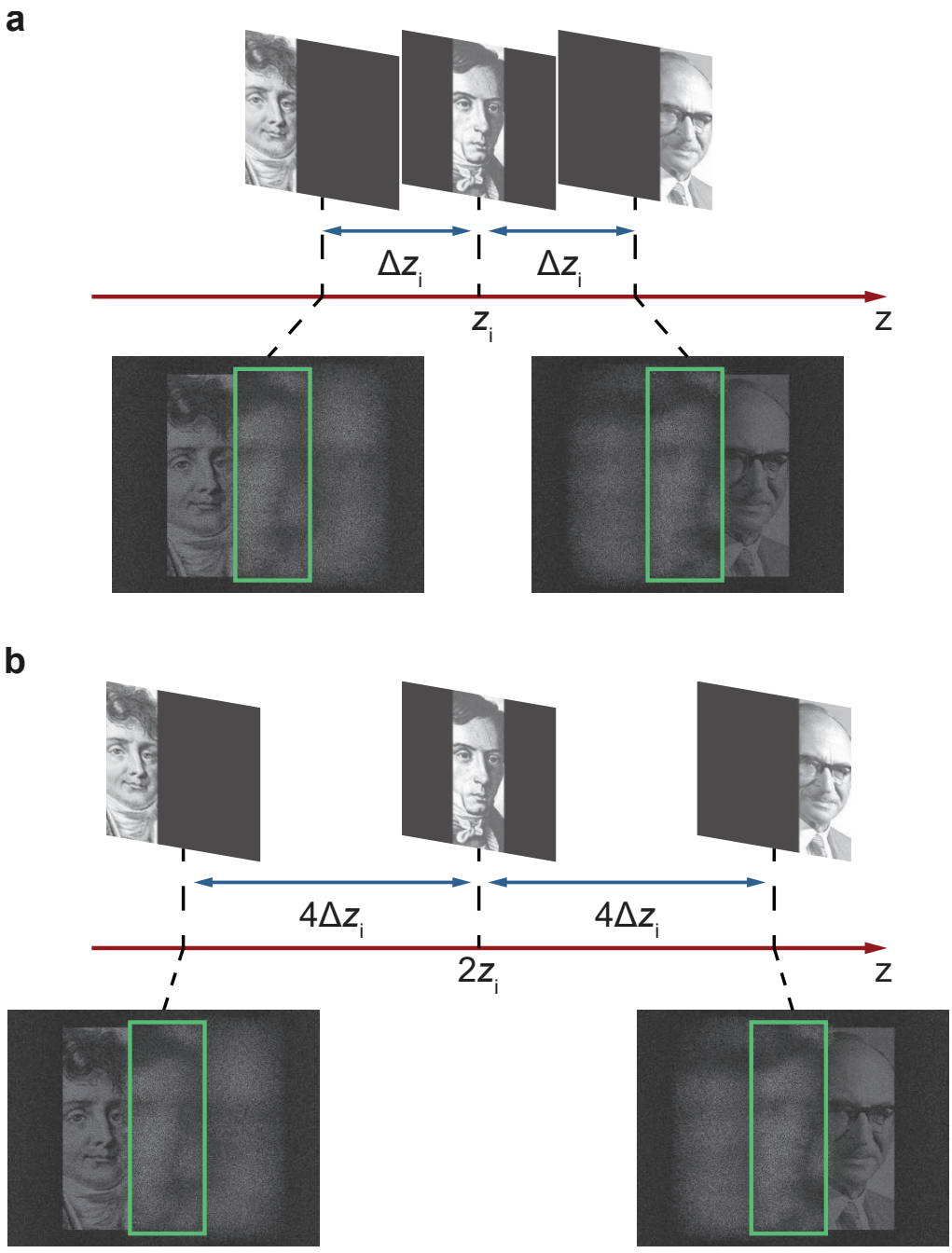

Supplementary Figure 4 Characterisation of axial resolution for 3D Fresnel holograms. Simulation results for two different Fresnel holograms, each projecting the same set of 3 images but at different distances. The portraits of Fourier, Fresnel, and Gabor are projected to **(a)** 19, 20, and 21 cm from the SLM; and **(b)** 36, 40, 44 cm, respectively, from the SLM. In both cases, the crosstalk from the central image is about the same, in agreement with the DoF expression.

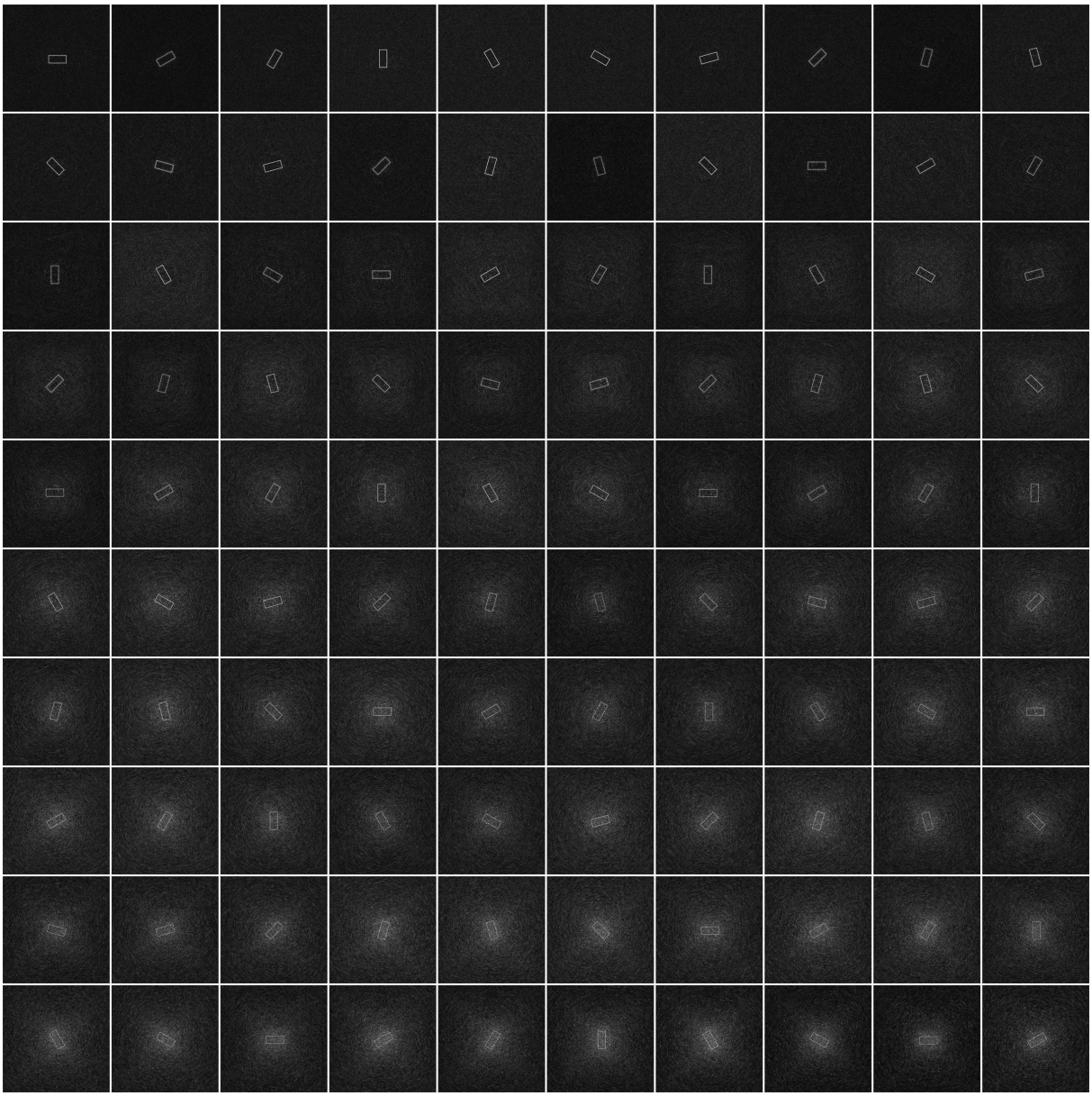

Supplementary Figure 5 Simulated images from a single 3D hologram are projected at 200 consecutive planes. Images are uniformly distributed over a distance of 50 cm, starting from 10 cm from the SLM (top left), and progressively increasing projection distance to 50 cm (lower right). The simulation assumes a 4000 × 4000 pixel CGH. The pixel size (20 μm) and illumination wavelength (1035 nm) are chosen the same as in the experiments given in Fig. 3. The presented images correspond only to the odd numbered ones, *i.e.*, 1, 3, ..199 in order to retain a reasonable size for the figure.

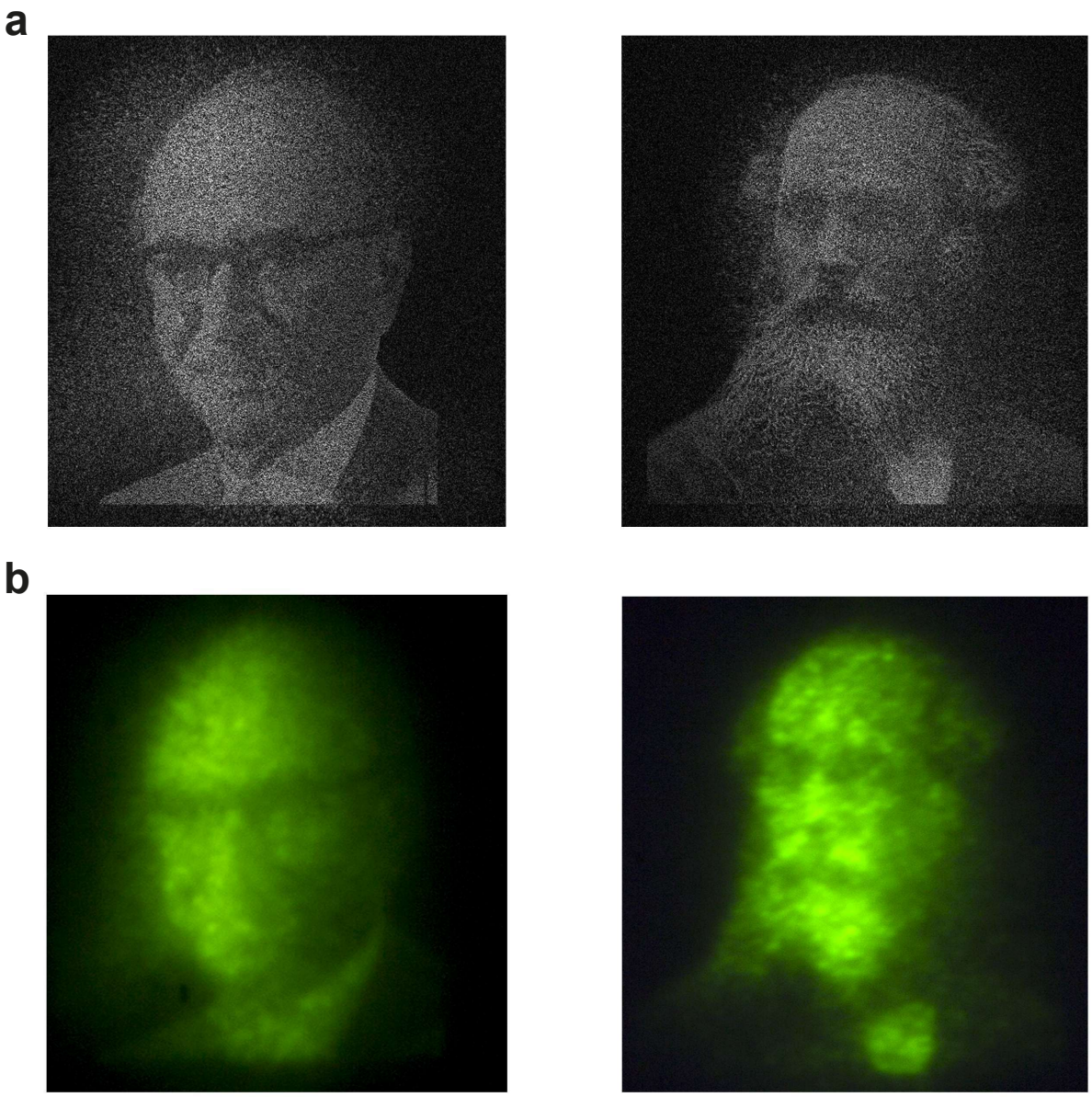

Supplementary Figure 6 Simulation and experimental results. (a) Simulation results of two back-to-back planes from a single Fresnel CGH. The hologram size is 512 × 512 pixels assuming a pixel size of 20 μm. **(b)** Experimental results from the same hologram in (a). The images are (left to right) 70 and 85.5 cm away from the hologram, after being relayed by a telescope.

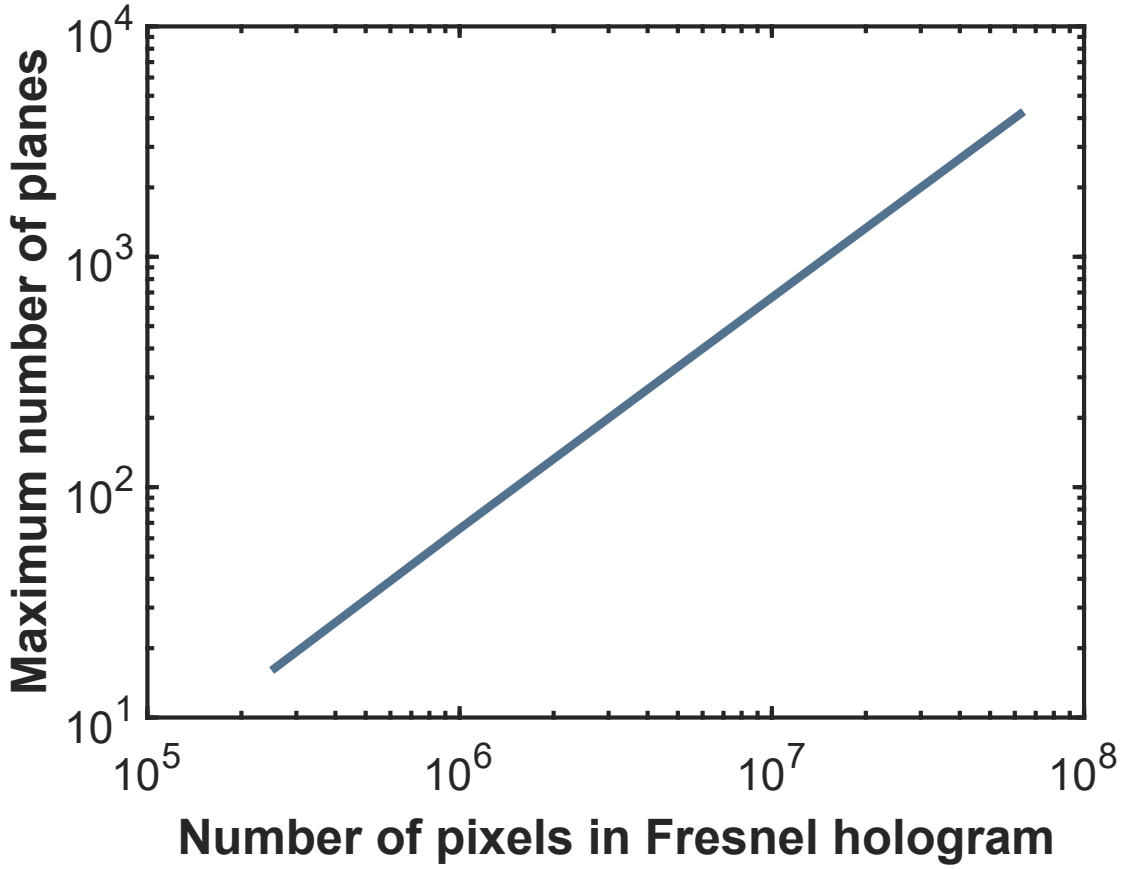

Supplementary Figure 7 Scaling of 3D holograms. The maximum number of projected planes with a single hologram as a function of hologram resolution, while keeping the image quality constant (RMSE ~ 0.24).

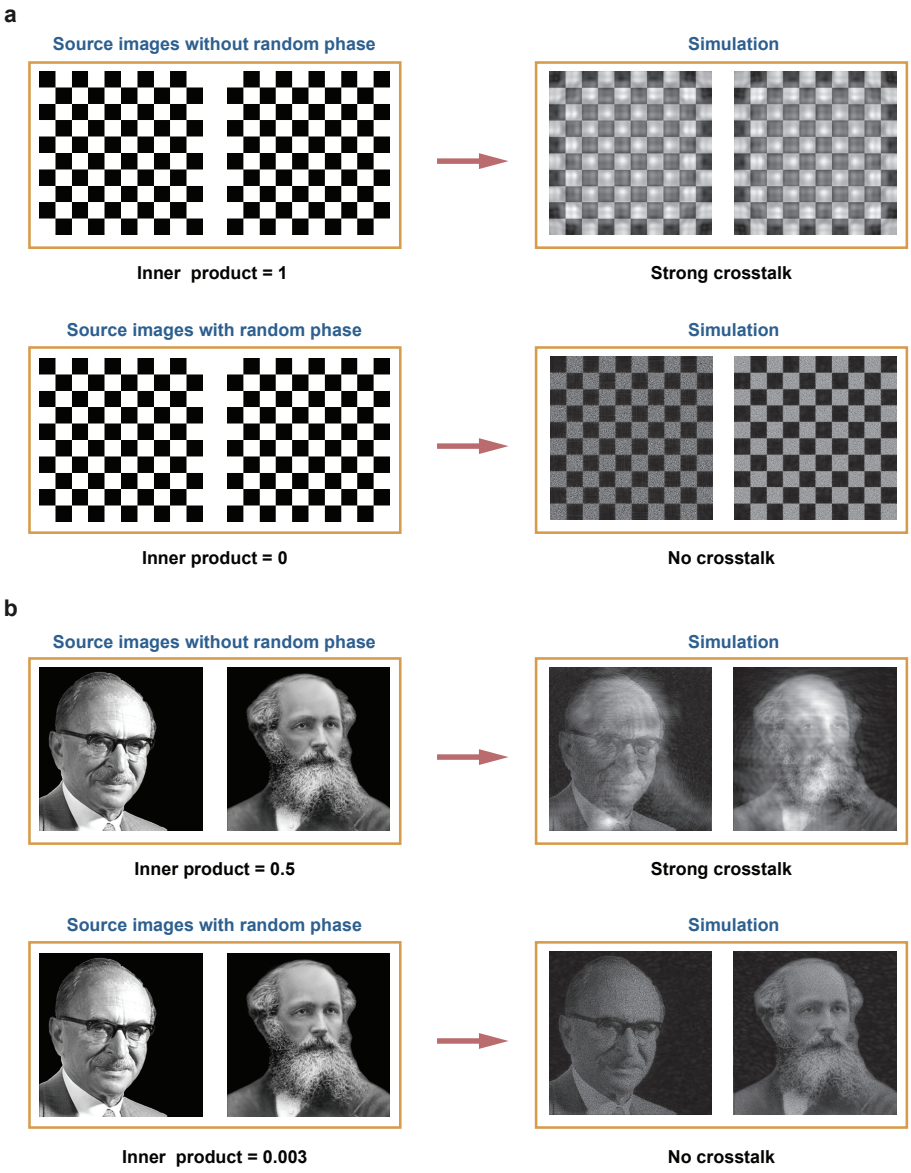

Supplementary Figure 8 The effect of random phase on crosstalk. (a) We first consider two simple images, namely, complementary checkerboard images, and calculate their inner product as a measure of their orthogonality. Then, we simulate projection of a hologram of these images. When the source images are supplied without random phase (with flat wavefront), the inner product value is about 1, and strong crosstalk is observed between the projected images at a given separation. When random phase is added to the source images, the inner product decreases to less than 10^{-3}, and the crosstalk between the projected images vanishes. **(b)** To show the generality of our approach, we repeat the steps in (a) with arbitrary images (portraits of Gabor and Maxwell), the inner product is 0.5 when no random phase is added, and the corresponding crosstalk is strong in the simulated projection. When a random phase added to both source images, the inner product becomes 0.003 and the crosstalk is absent in the simulation. The hologram size in all cases is 4000×4000 pixels.

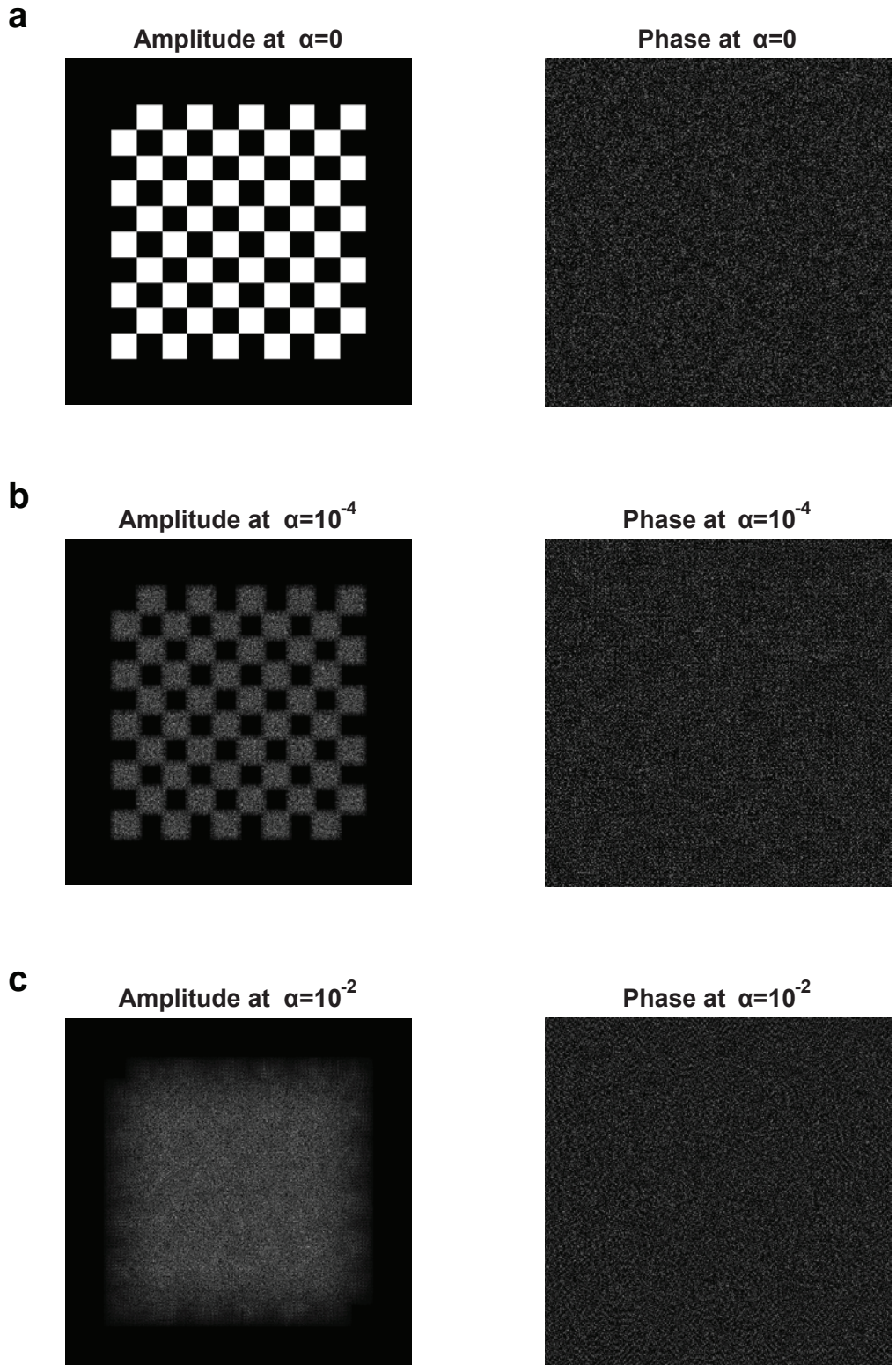

Supplementary Figure 9 Mixing of the random phase with amplitude through convolution with the parabolic wavefront. (a) The original field with the image encoded in amplitude (left) with random phase (right). **(b-c)** After convolution with a curved wavefront (nonzero α, corresponding to nonzero $|z_s - z_i|$), the amplitude (left) gets increasingly randomised as the value of α increases. The already random phase is also scrambled, leading lower average value. Here, blacks denote amplitude value of 0 and whites denote 1.

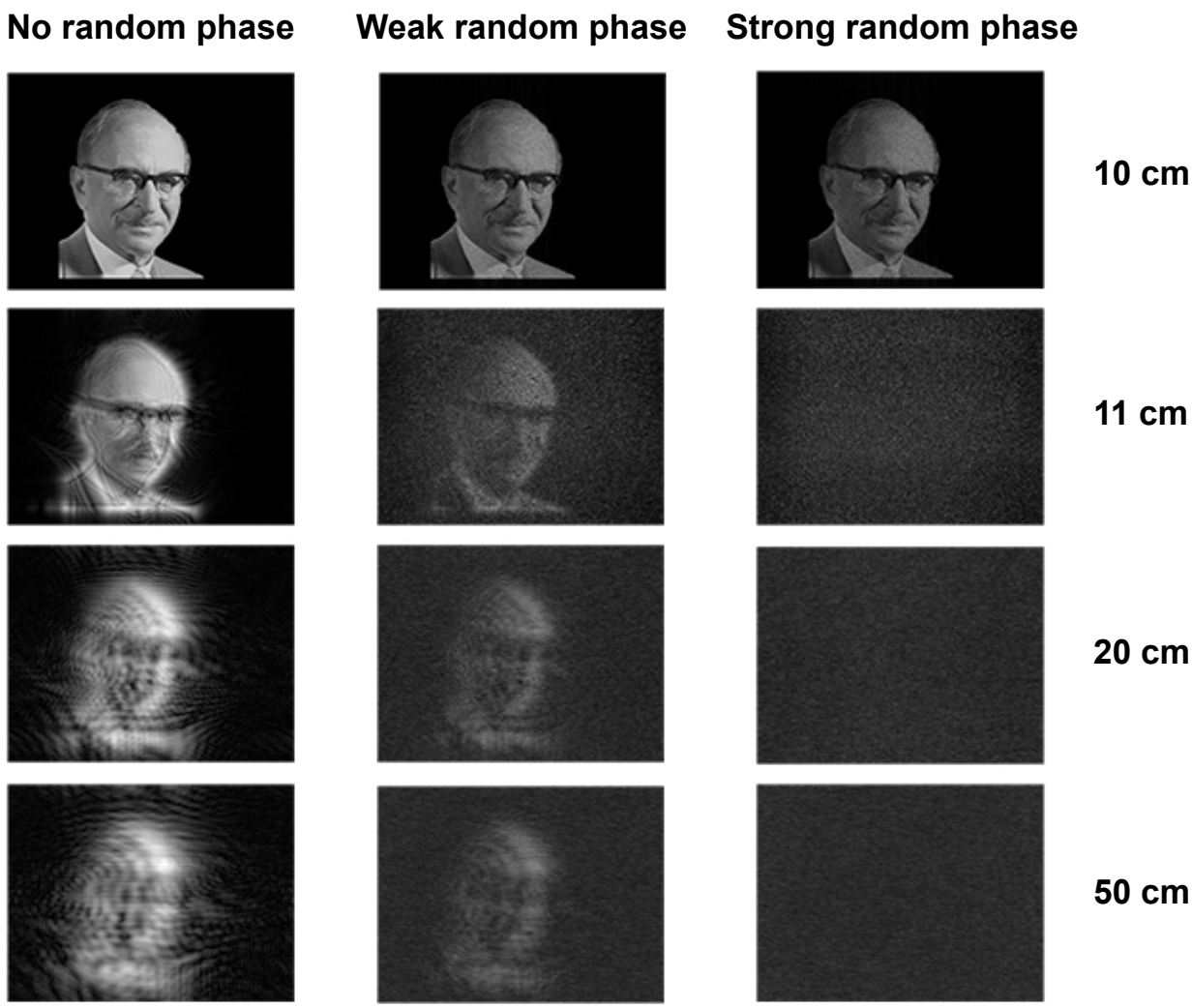

Supplementary Figure 10 Effect of the random phase on the crosstalk. The columns represent the effect of the random phase when the imaging plane is gradually removed from the projection plane for a given strength. Even a limited range of random phase (0 - 0.2π phase shift) shown in the middle column is sufficient to significantly decrease crosstalk. The effect of full random phase (0 - 2π phase shift) is shown in the last column, resulting in almost complete elimination of crosstalk.

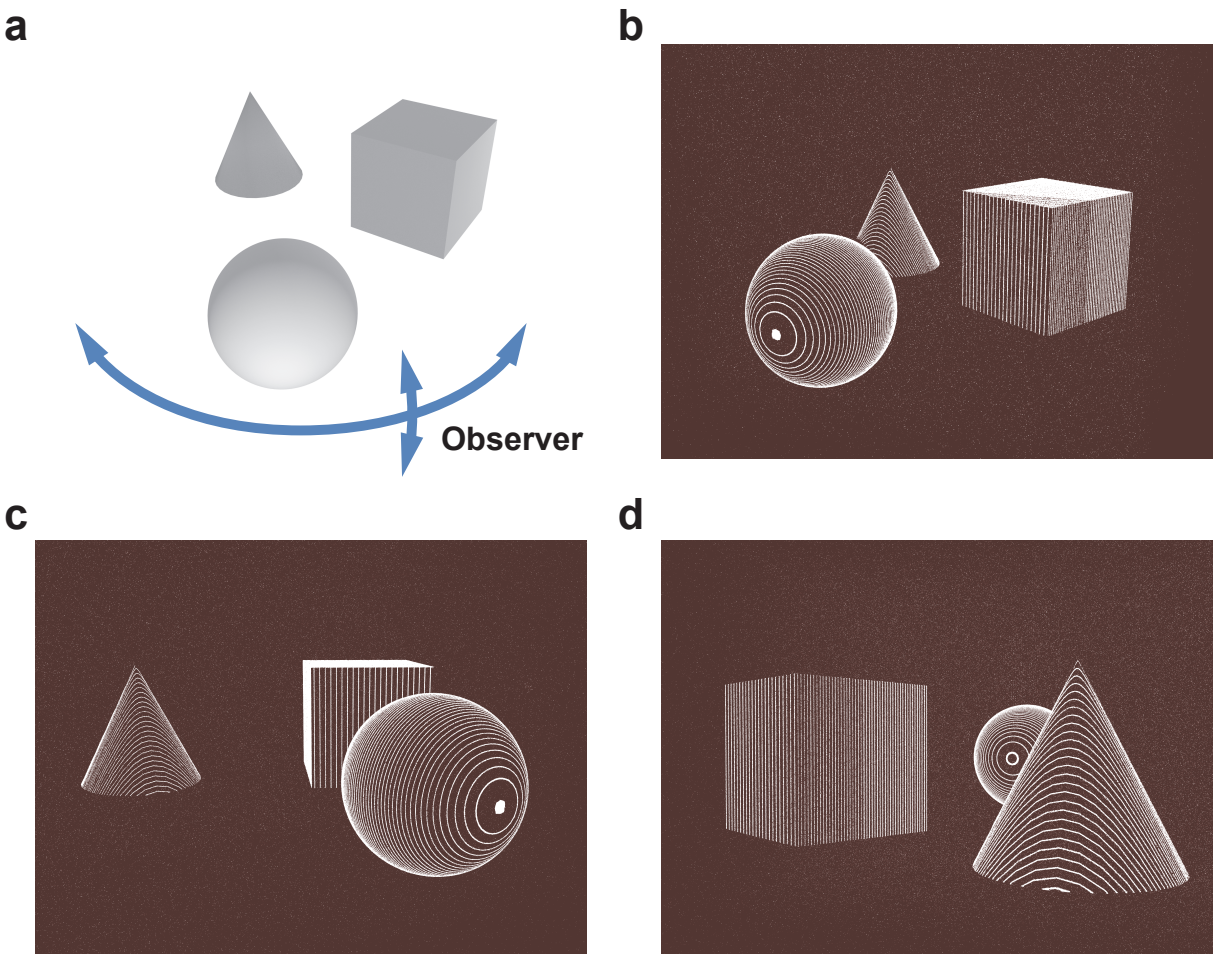

Supplementary Figure 11 Incorporation of occlusion cues. **(a)** 3D model of three objects chosen to illustrate occlusion. **(b-d)** The simulated projections viewed from three different positions.

References for the Supplementary Information

1. Fienup, J. R. Phase retrieval algorithms: a personal tour. *Appl. Opt.* **52**, 45-56 (2013).

2. Zhang, H., Cao, L. & Jin, G. Computer-generated hologram with occlusion effect using layer-based processing. *Appl. Opt*. **56**, F138-F143 (2017).

3. Askari, M., *et al*. Occlusion handling using angular spectrum convolution in fully analytical mesh based computer generated hologram. *Opt. Express* **25**, 25867-25878 (2017).

4. Liu, J.-P., Liao, H.-K. Fast occlusion processing for a polygon-based computer-generated hologram using the slice-by-slice silhouette method. *Appl. Opt.* **57**, A215-A221 (2018).